

J. J. Wiman · J. A. Sauls

Superfluid phases of ^3He in a periodic confined geometry*

February 15, 2020

Abstract Predictions and discoveries of new phases of superfluid ^3He in confined geometries, as well as novel topological excitations confined to surfaces and edges of near a bounding surface of ^3He , are driving the fields of superfluid ^3He infused into porous media, as well as the fabrication of sub-micron to nano-scale devices for controlled studies of quantum fluids. In this report we consider superfluid ^3He confined in a periodic geometry, specifically a two-dimensional lattice of square, sub-micron-scale boundaries (“posts”) with translational invariance in the third dimension. The equilibrium phase(s) are inhomogeneous and depend on the microscopic boundary conditions imposed by a periodic array of posts. We present results for the order parameter and phase diagram based on strong pair breaking at the boundaries. The ordered phases are obtained by numerically minimizing the Ginzburg-Landau free energy functional. We report results for the weak-coupling limit, appropriate at ambient pressure, as a function of temperature T , lattice spacing L , and post edge dimension, d . For all d in which a superfluid transition occurs, we find a transition from the normal state to a periodic, inhomogeneous “polar” phase with $T_{c_1} < T_c$ for bulk superfluid ^3He . For fixed lattice spacing, L , there is a critical post dimension, d_c , above which only the periodic polar phase is stable. For $d < d_c$ we find a second, low-temperature phase onsetting at $T_{c_2} < T_c$ from the polar phase to a periodic “B-like” phase. The low temperature phase is inhomogeneous, anisotropic and preserves time-reversal symmetry, but unlike the bulk B-phase has only D_{4h}^{L+S} point symmetry.

Keywords superfluid ^3He , confined quantum liquids, phase transitions

PACS numbers: 67.30.H-, 67.30.ej, 67.30.hp, 67.30.hr, 67.30.ht

* Published online in J. Low Temp. Phys. (2013) [doi: 10.1007/s10909-013-0924-4].

Department of Physics & Astronomy, Northwestern University, Evanston, IL 60208 USA
E-mail: jjwiman@u.northwestern.edu

1 Introduction

The p-wave, spin-triplet superfluid phases of ^3He provide the paradigm for unconventional BCS pairing in which spin- and orbital rotation symmetries, $\text{SO}(3)_s \times \text{SO}(3)_l$, are spontaneously broken in conjunction with $\text{U}(1)_N$ gauge symmetry. It was realized soon after the discovery that these broken symmetries, particularly parity and orbital rotation symmetry, implied that interfaces, boundaries and impurities could have profound effects on the superfluid phases.^{1,2} In the case of the bulk A-phase the effect of the boundary is to *lock* the orbital quantization axis, \hat{l} , normal to the boundary. The influence of boundaries can often extend to length scales much longer than the coherence length, $\xi_0 = \hbar v_f / 2\pi k_B T_c \approx 200 - 800 \text{ \AA}$ depending on pressure, when there is competition between alignment effects from curved boundaries and/or superflow.³ In a long cylinder with radius $R \gg \xi_0$ the boundary condition on \hat{l} leads to a *texture*, i.e. a long-wavelength spatial variation of the orbital quantization axis, \hat{l} , which is also an equilibrium current-carrying state.^{4,5,6} At the coherence length scale near a boundary strong pair-breaking typically occurs. The orbital component of the order parameter normal to the surface is suppressed and a spectrum of Fermionic states are localized near the boundary.^{7,8,9} The de-pairing effect of the boundary is further enhanced if the surface is rough on length scales comparable to or smaller than ξ_0 . If superfluid ^3He is confined to a region with dimensions of order a few coherence lengths then the geometry and surface structure on the boundaries can significantly modify the equilibrium phase diagram, and can even stabilize phases not realized in bulk superfluid ^3He .^{10,8,9,11}

Several studies of superfluid ^3He have been performed on thin films or within a slab geometry.^{12,13,14} In the case of strong one-dimensional confinement, i.e. boundary separation $D < D_{c_2} \approx 9\xi_0$, the A phase is expected to be the stable phase even at pressures well below the bulk critical pressure, $p_c \approx 21 \text{ bar}$.⁹ NMR measurements strongly support this prediction.¹⁵ This is in stark contrast to the bulk ^3He phase diagram in which the A phase is only stable at high temperature and pressure. In weak-coupling theory the planar and axial (ABM) phases are degenerate even with strong surface disorder.⁹ Strong-coupling effects which stabilize the ABM state at high pressures and high temperatures are poorly known for inhomogeneous phases at low-temperatures, $T \ll T_c$, and low pressures, $p \rightarrow 0 \text{ bar}$. For this reason the ground state of thin ^3He films at the lowest pressures is still an open question. At intermediate scales of confinement, $D_{c_2} < D < D_{c_1} \approx 13\xi_0$, the ground state in the weak-coupling limit is predicted to be a “crystalline” phase with an order parameter that spontaneously breaks translation symmetry in the plane of the film.¹¹ A one-dimensional periodic phase (“striped phase”) with in-plane wavelength $Q_{\perp}^{-1} \approx 3\xi_0$ has lower energy than any of the translationally invariant axial, planar or B-planar phases over a wide range of film thicknesses and temperatures. The mechanism responsible for spontaneously breaking translation symmetry for $D \lesssim D_{c_1}$ is the energy cost of surface pair-breaking compared to the energy cost for domain wall formation between degenerate B-planar phases. For $D < D_{c_1}$ it is energetically favorable for domain walls to enter the film. Interactions between domain walls lead to the striped phase. This type of competition between surface pair-breaking, the formation of topological defects and the stabilization of new phases not realized in bulk ^3He is part of the motivation for developing

sub-micron to nano-scale geometries for confining ${}^3\text{He}$.^{15,16} Of particular interest for this study is the possibility of confining ${}^3\text{He}$ in a periodic geometry such as a cavity supported by a periodic array of sub-micron scale posts.¹⁷

We break translational symmetry externally by considering ${}^3\text{He}$ infused into an infinite two-dimensional ($x-y$) periodic array of square posts, with translational invariance in the third dimension (z). This geometry can also be viewed as a two-dimensional ($2d$) grid formed of vertical (x) and horizontal (y) channels. The spatial region between the corners of four adjacent posts, or alternatively where the x and y channels intersect is particularly significant, and we will refer to this region as the ‘‘center’’ of the $2d$ cell when discussing superfluid ${}^3\text{He}$ confined within this structure. We expect the results reported here to be valid for confinement lengths in the z dimension, $L_z \gg 30\xi_0$.

The order parameter for superfluid ${}^3\text{He}$ belongs to the manifold of spin-triplet, p-wave, BCS pairing states represented by the 2×2 ‘‘gap matrix’’,

$$\hat{\Delta}(\hat{p}) = \sum_{\alpha i} (i\sigma_\alpha \sigma_y) A_{\alpha i} \hat{p}_i, \quad (1)$$

which is a function of the direction of relative momentum of the Cooper pair, \hat{p} , and is parametrized in its most general form by nine complex amplitudes, $A_{\alpha i}$. The 3×3 matrix order parameter transforms as a vector under spin rotations, and separately as a vector under orbital rotations. The maximal symmetry group for bulk ${}^3\text{He}$ is $G = U(1)_N \times SO(3)_S \times SO(3)_L \times P \times T$, where P , T and $U(1)_N$ represent space inversion, time-reversal and global gauge symmetries of the normal phase. The symmetry reduction resulting from the weak nuclear dipolar interaction is omitted here, but is important in resolving relative spin-orbit rotational degeneracies, and in determining the NMR signatures of the phases of confined ${}^3\text{He}$.

2 Ginzburg-Landau Theory

To determine the phase diagram and superfluid order parameter for ${}^3\text{He}$ confined within a $2d$ periodic structure we minimize the Ginzburg-Landau (GL) free energy for a general spin-triplet, p-wave condensate defined as a functional of the 3×3 matrix order parameter. A few atomic units away from a boundary the ${}^3\text{He}$ - ${}^3\text{He}$ interactions responsible for pairing are invariant under the maximal symmetry group of bulk ${}^3\text{He}$. Thus, the GL functional takes its bulk form,^{18,19}

$$\begin{aligned} \Omega[A] = \int_V d\mathbf{R} \left\{ \alpha(T) \text{Tr}(AA^\dagger) + \beta_1 |\text{Tr}(AA^T)|^2 + \beta_2 [\text{Tr}(AA^\dagger)]^2 \right. \\ \left. + \beta_3 \text{Tr}[AA^T(AA^T)^*] + \beta_4 \text{Tr}[(AA^\dagger)^2] + \beta_5 \text{Tr}[AA^\dagger(AA^\dagger)^*] \right. \\ \left. + K_1 (\nabla_k A_{\alpha j} \nabla_k A_{\alpha j}^*) + K_2 (\nabla_j A_{\alpha j} \nabla_k A_{\alpha k}^*) + K_3 (\nabla_k A_{\alpha j} \nabla_j A_{\alpha k}^*) \right\}. \end{aligned} \quad (2)$$

The equilibrium order parameter is obtained from the stationarity condition for the GL functional. Confinement is introduced via boundary conditions of the order parameter field, $A_{\alpha i}(\mathbf{R})$. For ${}^3\text{He}$ confined in a non-magnetic, periodic geometry with 4-fold rotational, reflection and inversion symmetries, the maximal symmetry

group is reduced by restricting the orbital rotations to the point group D_{4h} (which includes space inversion), i.e.

$$G = U(1)_N \times SO(3)_S \times D_{4h} \times T. \quad (3)$$

The domain, V , is a square unit cell with side length L . Periodic boundary conditions are imposed on the order parameter field at the outer boundaries of this unit cell. In the interior of the unit cell is an inner boundary representing the square post of side length d . Typical boundary conditions for the order parameter on the inner boundary are: (i) *maximal* pair-breaking in which all components of the order parameter vanish on the inner boundary and (ii) *minimal* pair-breaking in which only the orbital component normal to the surface of the inner boundary is forced to vanish, and the normal derivative of the tangential orbital components vanishes on the inner boundary. This latter boundary condition corresponds to surfaces with specular reflection,¹ while the former boundary condition corresponds to an atomically rough surface with strong backscattering.²⁰ Here we report results based on maximal pair-breaking. We numerically minimize the GL functional on this domain, and determine the stable (and in some cases meta-stable) order parameter (phases) for superfluid ^3He in this class of periodic confined geometries. We also present results for the phase diagram as a function of temperature T , confinement length $D \equiv L - d$, and period L . The results reported here are appropriate for low pressures in the GL regime. Thus, we assume weak-coupling values for the GL material parameters:^{18,19}

$$\alpha(T) = \frac{1}{3}N(0)(T/T_c - 1), \quad 2\beta_1 = -\beta_2 = -\beta_3 = -\beta_4 = \beta_5, \\ K_1 = K_2 = K_3 = \frac{3}{5}N(0)\xi_0^2, \quad \beta_1 = -\frac{N(0)}{(\pi k_B T_c)^2} \left\{ \frac{1}{30} \left[\frac{7}{8} \zeta(3) \right] \right\}, \quad (4)$$

where T_c is the superfluid transition temperature for bulk ^3He , ξ_0 is the zero-temperature correlation length, and $N(0) = k_f^3/2\pi^2 v_f p_f$ is the single-spin quasi-particle density of states at the Fermi surface, defined in terms of the Fermi velocity, v_f , and Fermi momentum and wavenumbers, $p_f = \hbar k_f$.

In what follows we neglect the nuclear dipolar energy and choose *aligned* spin and orbital coordinate axes, $\{x, y, z\}$, corresponding to the high symmetry directions of the periodic channel. Thus, the order parameter is represented by,

$$A = \begin{pmatrix} A_{xx} & A_{xy} & A_{xz} \\ A_{yx} & A_{yy} & A_{yz} \\ A_{zx} & A_{zy} & A_{zz} \end{pmatrix}. \quad (5)$$

For bulk ^3He , the B-phase, defined by the Balian-Werthamer state,

$$A^B = \frac{\Delta_B}{\sqrt{3}} \begin{pmatrix} 1 & 0 & 0 \\ 0 & 1 & 0 \\ 0 & 0 & 1 \end{pmatrix}, \quad (6)$$

with amplitude given by

$$\Delta_B^2(T) = \frac{1}{2} \frac{|\alpha(T)|}{\beta_{12} + \frac{1}{3}\beta_{345}}, \quad (7)$$

is the equilibrium phase at low pressures with free energy density given by

$$\Omega_{\text{B}}/V = -\frac{1}{4} \frac{|\alpha(T)|^2}{\beta_{12} + \frac{1}{3}\beta_{345}} = -\frac{\Delta C_{\text{B}}}{2T_c} (T - T_c)^2. \quad (8)$$

The second term is the B-phase condensation energy scaled in terms of the heat capacity jump, ΔC_{B} , at the normal to B-phase transition. For weak-coupling values of the material coefficients this gives the BCS result, $\Delta C_{\text{B}}/C_{\text{N}} = 12/7\zeta(3) \simeq 1.43$, where $C_{\text{N}} = \frac{2}{3}\pi^2 N(0)T_c$ is the normal-state heat capacity at T_c . These values for the bulk B-phase order parameter and free energy are used as the scale for the order parameter and free energy of confined ^3He .

We note that the boundary condition imposed by the interior post is expected to be accurate only for post side lengths $d \gtrsim \xi_0$. For post dimensions, $d \ll \xi_0$, the boundary is more accurately treated microscopically as an ‘‘impurity’’ that scatters excitations and breaks pairs.² The pair-breaking effect of an impurity with side dimension smaller than a coherence length is reduced by d/ξ_0 near the post. We avoid this limit and restrict our analysis to post dimensions with $d \geq \frac{1}{2}\xi_0$.

Before discussing the numerical results we describe some of the possible phases with a high degree of residual symmetry, i.e. sub-groups of the maximal symmetry group, that may be realized by ^3He in a confined $\text{D}_{4\text{h}}$ geometry.

3 Symmetry Classes of ^3He in a confined $\text{D}_{4\text{h}}$ geometry

The effects of confinement are enforced by the boundary conditions imposed on the order parameter. The boundary conditions reflect the point symmetry of the confining boundaries. For the case of a periodic array of square posts the elementary symmetry group of a square post, $\text{C}_{4\text{v}}$, is the combined set of four-fold rotations, $\{E, C_4, C_4^2, C_4^3\}$, where E is the identity and $C_4^n = (C_4)^n$ is a rotation about the z axis by $n \times \pi/2$, the set of reflections through four vertical planes, $\{\Pi_{zx}, \Pi_{zy}, \Pi_{zx'}, \Pi_{zy'}\}$, and the corresponding rotary reflections, $\{R_{zi} \equiv C_4 \Pi_{zi} \mid i = x, y, x', y'\}$, where (x', y') are axes rotated from (x, y) by $\pi/4$ about z . The addition of reflection symmetry through the horizontal plane, Π_{xy} , and 180° rotations about the vertical plane symmetry axes, $\{C_{2x}, C_{2y}, C_{2x'}, C_{2y'}\}$, defines the point group, $\text{D}_{4\text{h}}$, which includes space inversion, $C_i = C_{2y} \cdot \Pi_{zx}$.

For any element $g \in \text{D}_{4\text{h}}$ a scalar function transforms as $f(\mathbf{R}) \xrightarrow{g} f(\hat{g}^T \cdot \mathbf{R})$, where \hat{g} is the 3×3 matrix representing the symmetry element g , $\hat{g}^T = \hat{g}^{-1}$ is the matrix inverse, and $\mathbf{R} = (x, y)$. Thus, the order parameter field, which is a vector under space rotations and reflections, transforms as $A_{\alpha i}(\mathbf{R}) \xrightarrow{g} g_{ij} A_{\alpha j}(\hat{g}^T \cdot \mathbf{R})$. Similarly, for any rotation $g \in \text{SO}(3)_{\text{s}}$ we have, $A_{\alpha i}(\mathbf{R}) \xrightarrow{g} g_{\alpha\beta} A_{\beta i}(\mathbf{R})$, and under a gauge transformation, $\chi \in \text{U}(1)_{\text{N}}$, $A_{\alpha i}(\mathbf{R}) \xrightarrow{\chi} e^{-i\chi} A_{\alpha i}(\mathbf{R})$. Time-reversal, T , reduces to complex conjugation, $A_{\alpha i}(\mathbf{R}) \xrightarrow{\text{T}} A_{\alpha i}^*(\mathbf{R})$.

3.1 Non-Equal Spin Pairing - The B_{\square} Phase

In the case of bulk ^3He the maximal symmetry sub-group of joint spin and orbital rotations combined with time-reversal, $\text{SO}(3)_{\text{L+S}} \times \text{T}$, is the symmetry class of the

B-phase, i.e. the Balian-Werthamer state with $A_{\alpha i}^{\text{BW}} = \Delta \delta_{\alpha i}$. The *discrete analog* of the bulk B-phase is a state, which we refer to as the B_{\square} -phase, that is invariant under joint spin and orbital elements of the maximal point group, D_{4h} , and time-reversal, i.e. $H_{B_{\square}} = D_{4h}^{\text{L+S}} \times T$. Note that space inversion is broken, but space inversion combined with inversion in spin-space is a symmetry of the B_{\square} -phase.

The matrix structure of the B_{\square} order parameter differs substantially from the isotropic B -phase. For all $g \in H_{B_{\square}}$, the order parameter satisfies,

$$A_{\alpha i}(\mathbf{R}) \xrightarrow{g} g_{\alpha\beta} A_{\beta j}(\hat{g}^T \cdot \mathbf{R}) g_{ji}^T = A_{\alpha i}(\mathbf{R}). \quad (9)$$

It is then straightforward to show that

$$A^{B_{\square}} = \begin{pmatrix} A_{xx} & A_{xy} & 0 \\ A_{yx} & A_{yy} & 0 \\ 0 & 0 & A_{zz} \end{pmatrix}, \quad (10)$$

with $A_{xx}(x, y) = A_{yy}(y, x)$, $A_{xy}(x, y) = A_{yx}(y, x)$, $A_{zz}(x, y) = A_{zz}(y, x)$ and all components are real (T symmetry). The diagonal (off-diagonal) components are even (odd) under $x \rightarrow -x$ or $y \rightarrow -y$. The numerical results presented below show that the B_{\square} -phase is the equilibrium state in the weak-coupling limit at low temperatures.

3.2 Equal Spin Pairing States

The superfluid phases with the highest degree of residual symmetry are those that preserve a continuous rotation symmetry about an axis \hat{d} in spin space, i.e. $SO(2)_{\text{sd}}$. The direction \hat{d} is a vector representing spontaneously broken spin-rotation symmetry. If \hat{d} is real, then the broken symmetry phase is an equal-spin-pairing (ESP) state and \hat{d} is the direction in which the Cooper pairs have zero spin projection. The residual symmetry group of the class of ESP states includes $SO(2)_{\text{sd}} \times Z_2^{\text{spin}}$, where $Z_2^{\text{spin}} = \{1, e^{i\pi} R_{\pi\hat{x}}^{\text{spin}}\}$ is a two element group of the identity and the combined operation of a gauge transformation, $e^{i\pi}$, and a rotation of π about an axis $\hat{x} \perp \hat{d}$ in spin space. Continuous $U(1)_{\text{N}}$ symmetry is broken, but elements of $U(1)_{\text{N}}$ may be combined with spin or orbital rotations and reflections. In particular, the point symmetry, D_{4h} , is necessarily broken by any p-wave pairing state. However, the residual symmetry of the z-aligned polar (P_z) phase contains all the elements of D_{4h} . In particular, the P_z phase can be expressed as $A_{\alpha i}^{P_z} = \hat{d}_{\alpha} a(x, y) \hat{z}_i$ with $a(x, y)$ real (time-reversal symmetry) and invariant under the sub-group C_{4v} : $a(x, y) = a(y, x) = a(-x, y) = a(x, -y)$. The P_z order parameter undergoes a sign change for any of the C_{2i} operations and reflection in the xy plane since $\hat{z} \rightarrow -\hat{z}$. Thus, combining these operations with the gauge transformation, $e^{i\pi}$, and C_{4v} yields the group, $D_{4h}^{\text{L},\pi}$, which is isomorphic to D_{4h} . Thus, the residual symmetry group for the P_z phase is

$$H_{P_z} = SO(2)_{\text{sd}} \times Z_2^{\text{spin}} \times D_{4h}^{\text{L},\pi} \times T. \quad (11)$$

This state is the stable superfluid phase that onsets from the normal state at T_{c1} .

The P_z phase retains the sub-group C_{4v} of point symmetries, but is not the only ESP state with this symmetry. If we omit the operations that transform $z \rightarrow -z$, then we obtain two possible symmetry classes. If time-reversal is preserved we obtain the residual symmetry group is

$$H_{3D} = SO(2)_{S_d} \times Z_2^{\text{spin}} \times C_{4v}^L \times T \quad (12)$$

with an orbital order parameter field, $\mathbf{a} = a_x \hat{x} + a_y \hat{y} + a_z \hat{z}$, that includes three real components satisfying the reflection symmetries,

$$a_x(x, y) = -a_x(-x, y) = +a_x(x, -y) \quad (13)$$

$$a_y(x, y) = +a_y(-x, y) = -a_y(x, -y) \quad (14)$$

$$a_x(x, y) = a_y(y, x) \quad (15)$$

$$a_z(x, y) = a_z(y, x) = a_z(-x, y) = a_z(x, -y). \quad (16)$$

This phase is not found to be a local minimum of the GL functional for the weak-coupling values of the β parameters.

Another ESP phase with C_{4v}^L symmetry is obtained if we break T symmetry, but preserve $\Pi_{xy} \cdot T$. In this case the residual symmetry group is

$$H_{\text{chiral}-C_{4v}} = SO(2)_{S_d} \times Z_2^{\text{spin}} \times C_{4v}^L \times \{E, \Pi_{xy} \cdot T\}. \quad (17)$$

The orbital vector, $\mathbf{a}_{\pm} = \mathbf{a}_{\perp} \pm ia_z \hat{z}$, with $\mathbf{a}_{\perp} = a_x \hat{x} + a_y \hat{y}$, is a complex vector field with real amplitudes $\{a_x, a_y, a_z\}$ satisfying the reflection symmetries in Eqs. 13-16 required by C_{4v}^L . The \pm sign reflects the two-fold degeneracy resulting from broken time-reversal symmetry. These are *chiral* phases with a local chiral vector field given by

$$\mathbf{l}_{\pm} = \pm \mathbf{a}_{\perp} \times a_z \hat{z} = \pm a_z(\mathbf{R}) [a_y(\mathbf{R}) \hat{x} - a_x(\mathbf{R}) \hat{y}], \quad (18)$$

which is confined to the xy plane. For a unit cell centered on the post, the chiral vector vanishes on the post boundaries and at the center of the two channels, where $a_x = a_y = 0$, if the periodicity of the ordered phase is the same as that of the underlying geometry. Here the phase is locally the P_z phase. For chiral phases, and more generally current carrying states, the periodicity of the ordered phase need not equal the underlying lattice periodicity. Thus, a complete classification of the residual symmetry sub-groups should include the space-group operations. This is beyond the scope of this report, but underscores the complexity of the possible phases of ${}^3\text{He}$ in a periodically confined geometry. In the weak-coupling limit this chiral ESP phase is not energetically stable, but this phase, or a closely related phase with period $2L$, may emerge as a stable, or meta-stable, low temperature phase at high pressures due to strong coupling effects.¹ However at high pressures, for very weak confinement, $L \gg 20\xi_0$, and small post dimensions, $d \lesssim \xi_0$, the chiral $-C_{4v}^L$ phase is unlikely to be the equilibrium phase. In this limit we expect a chiral ABM-like phase with $\mathbf{l} \parallel \hat{z}$ in the center of the channels to be the equilibrium phase at temperatures below a narrow region of stability of the P_z phase.

¹ The in-plane chiral phase with period $2L$ is a periodic version of the texture obtained by Surovtsev and Fomin²¹ for a uniform distribution of rod-like impurities embedded in ${}^3\text{He-A}$.

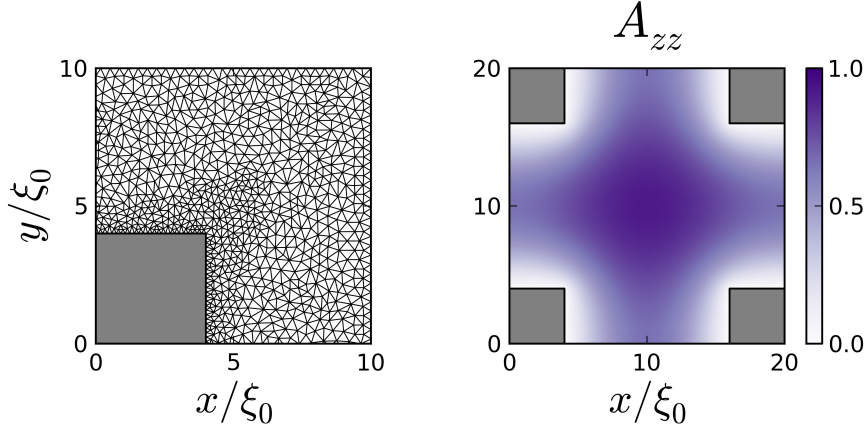


Fig. 1 (Color online) Left panel: One-fourth of the unit cell showing the triangular computational grid. The grey region defines the area occupied by the post. Right panel: Order parameter amplitude, $A_{zz}(\mathbf{R})$, of the z-aligned Polar phase for $L = 20\xi_0$, $d = 8\xi_0$, $T = 0.9T_c$, and $\hat{d} = \hat{z}$. The order parameter is real and scaled in units of the bulk B-phase order parameter, $\Delta_B(T)$.

The residual symmetries that define the bulk ABM phase, $A_{\alpha i}^{\text{ABM}} = d_\alpha (\hat{m} \pm i\hat{n})_i$, are (i) *chiral symmetry*, $Z_2^{\text{chiral}} = \{E, P_2 \cdot T\}$, where P_2 is reflection in a plane containing the chiral axis $\hat{l} = \hat{m} \times \hat{n}$, and (ii) *gauge-orbit symmetry*, $U(1)_{L_z - N}$, i.e. rotation by angle ϑ about the chiral axis, combined with a gauge transformation, $e^{\pm i\vartheta}$, by phase angle $\mp\vartheta$. A discrete analog of the ABM phase of bulk ${}^3\text{He}$ is obtained by breaking C_{4v}^L rotational symmetry, but restoring symmetry with appropriate elements from $U(1)_N$. In addition, T symmetry is broken, but chiral symmetry is present as invariance with respect to the combined operation, $T \cdot \Pi_{zx}$. Thus, the discrete ABM phase is invariant with respect to the group obtained from these generators,

$$C_{4h}^{\text{L-N,T}} = \left\{ E, e^{i\pi/2} C_4, e^{i\pi} C_4^2, e^{i3\pi/2} C_4^3, T\Pi_{zx}, e^{i\pi/2} T\Pi_{zx'}, e^{i\pi} T\Pi_{zy}, e^{i3\pi/2} T\Pi_{zy'} \right\}, \quad (19)$$

and is isomorphic to C_{4v}^L . The full symmetry group is then

$$H_{A_\square} = \text{SO}(2)_{S_d} \times Z_2^{\text{spin}} \times C_{4h}^{\text{L-N,T}}, \quad (20)$$

and the functional form of the discrete ABM phase is $A_{\alpha i}^\pm = a(x, y) \hat{d}_\alpha (\hat{x} \pm i\hat{y})_i$, where $a(x, y)$ is real and obeys the C_{4v}^L reflection symmetries in Eq. 16. The A_\square -phase is not stable in the weak-coupling limit. However, several chiral phases are found to be stationary points of the GL functional for strong-coupling values of the β -parameters appropriate for high pressures. The phase diagram at high pressures will be discussed in a separate report.

4 Numerical Methods

To compute the order parameter which minimizes the GL functional we implement a finite element method (FEM).²² We discretize the ${}^3\text{He}$ unit cell with an

unstructured triangular mesh generated with the code `Triangle`.²³ This type of mesh permits spatially varying triangular element sizes, which we use to provide finer spatial resolution in regions near boundaries and sharp corners as shown in the left panel of Fig. 1. Also, an unstructured mesh does not enforce any point symmetry that a periodic mesh possesses. Thus, the residual symmetries of the phases we find result from interaction terms in the GL functional combined with pair-breaking and periodicity represented by the boundary conditions.

For the FEM we represent the order parameter with quadratic Lagrange interpolating functions defined on each element. The Lagrange interpolating functions are determined by the values of the order parameter at six nodes corresponding to the vertices and midpoints of edges of each element. The order parameter field defined at the nodes of each element is continuous across the entire domain. The resulting integration over the domain then separates into independent integrals over each element which we evaluate numerically with Gauss-Legendre quadrature.²⁴

We minimize the discretized GL functional using an implementation of the conjugate gradient algorithm, `CG_DESCENT`.²⁵ The gradient, $\mathbf{G}[A] \equiv \delta\Omega/\delta A^\dagger(\mathbf{R})$, is evaluated at each node within the finite element scheme and input as the gradient in the conjugate gradient method. We set convergence as $\max\{|\mathbf{G}_i[A]|\} < 10^{-7}$, for all i degrees of freedom (i.e. all 9 complex components of A at each node) which we determined to yield no significant loss of accuracy compared to stricter tolerances.

5 Stable Phases - Maximal Pair-breaking

Figure 1 (right panel) shows the equilibrium order parameter for confined ${}^3\text{He}$ with period $L = 20\xi_0$ and post dimension $d = 8\xi_0$ at temperature $T = 0.9T_c$ for the case of maximal pair-breaking by the interior boundary. This is a spatially modulated z -aligned Polar (P_z) state in which only the z -orbital component, A_{zz} , is non-vanishing. This phase breaks spin- and orbital rotation symmetry, but preserves time-reversal symmetry. Note that the polar amplitude is maximum in the center of the channel and decreases by approximately 50% into both x - and y channels. The P_z phase is an equal-spin pairing state and thus the more general representation for this phase is $A_{\alpha i} = \Delta(\mathbf{R})\hat{d}_\alpha\hat{z}_i$, where \hat{d} is a real unit vector that defines the broken rotational symmetry in spin space. The P_z phase with only $A_{zz} \neq 0$ corresponds to $\hat{d} = \hat{z}$, and is degenerate with respect to the orientation of \hat{d} since we have neglected the nuclear dipole and Zeeman energies. The P_z phase belongs to the symmetry class of pairing states defined by the sub-group, $H_{P_z} = \text{SO}(2)_{\text{sd}} \times \text{Z}_2^{\text{spin}} \times \text{D}_{4h}^{L,\pi} \times \text{T}$, as discussed in Sec. 3

For the periods, $L \leq 30\xi_0$, and temperatures within the region of stability of the P_z phase, we find a finite Polar amplitude everywhere within the ${}^3\text{He}$ cavity, except at the post boundaries. However for much larger periods, L , and the same channel width, $D = L - d$, the amplitude of the P_z order parameter appears to vanish deep within the x - and y channels far from the center, leaving a lattice of isolated islands of P_z condensate in the center. This suggests there may be a regime in which decoupled P_z condensates nucleate in the center region, but are not phase coherent and do not exhibit superfluidity.

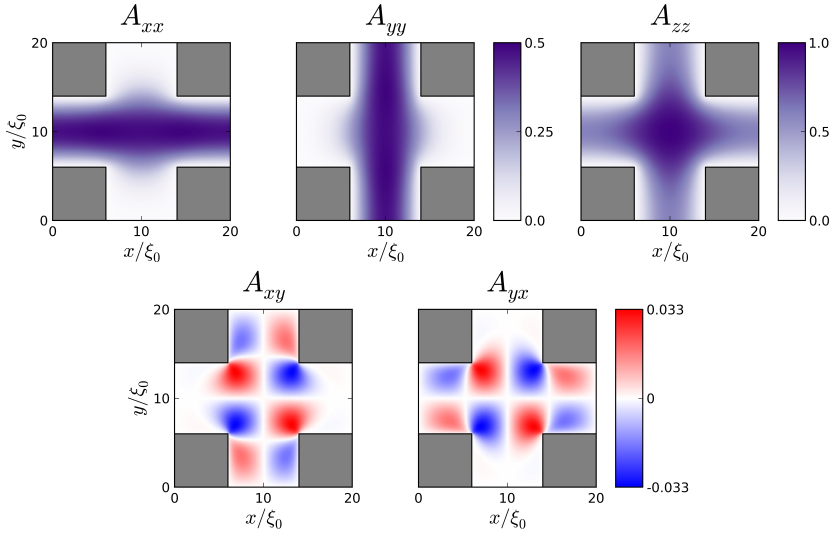


Fig. 2 (Color online) Order parameter components of the B_{\square} phase plotted in the domain V for $L = 20\xi_0$, $d = 12\xi_0$, and $T = 0.7T_c$. All values are real and scaled by the bulk B-phase order parameter $\Delta_B(T)$. Note the reduced scale of the A_{xy} amplitude.

For the same period, post dimension and boundary conditions we also find a second stable phase in the weak-coupling regime at a lower temperature. This phase (B_{\square}) also preserves time-reversal symmetry, but has lower symmetry than that of the P_z phase. The B_{\square} phase is similar to the bulk B-phase in that the order parameter is real, with diagonal elements, A_{xx} , A_{yy} and A_{zz} in the center of the channel as shown in Fig. 2. However, the component A_{xx} (A_{yy}) is strongly suppressed in the y -channel (x -channel), and off-diagonal components, A_{xy} and A_{yx} , appear at the corners of the posts. It is also clear from Fig. 2 that the components of the order parameter obey the reflection symmetries: $A_{xx}(x, y) = A_{yy}(y, x)$ and $A_{xy}(x, y) = A_{yx}(y, x)$, and that the diagonal components, A_{xx} , A_{yy} and A_{zz} are even functions of x and y , while the off-diagonal components, A_{xy} and A_{yx} , are odd under $x \rightarrow -x$ or $y \rightarrow -y$. The remaining off-diagonal components are all zero: $A_{zx} = A_{xz} = A_{zy} = A_{yz} = 0$. As discussed in Sec. 3 these are the conditions imposed by the discrete sub-group, $H_B = D_{4h}^{L+S} \times T$. This is the maximal allowed point symmetry and is the discrete analog of the maximal subgroup $SO(3)_{L+S}$ for the bulk B-phase. Indeed, we recover the bulk B-phase for $L \rightarrow \infty$ and $d \rightarrow 0$, as indicated in Fig. 3. Note that the off-diagonal components are significantly smaller in magnitude than the diagonal components and become negligible far from the post corners, except for $D \approx D_c(T)$, the critical line separating the P_z and B_{\square} phases.

The phase transition from the P_z to B_{\square} phase is presented in Fig. 3, which shows the maximal magnitudes for the components of the order parameter as a function of the confinement length D/ξ_0 for fixed period, L , and temperature, T . The transition is 2nd order, i.e. continuous as a function of D or T , with spontaneously broken symmetry from $H_{P_z} \rightarrow H_{B_{\square}}$. For confinement lengths onsetting at the critical value, $D_c(T) \rightarrow 4.1\xi_0$ at $T = 0$ and $L = 20\xi_0$, the x and y components,

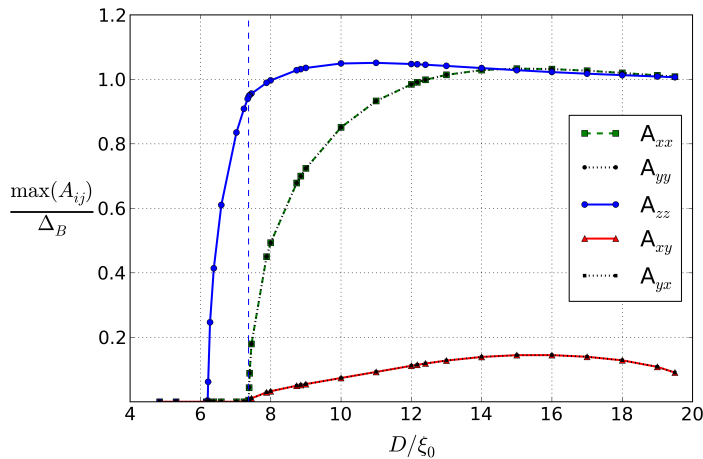


Fig. 3 (Color online) Order parameter amplitude as a function of the confinement length, D , for $L = 20\xi_0$ and $T = 0.7T_c$. The amplitudes are taken as the maxima within the domain. Note that maxima for A_{xx} and A_{yy} are equal, as are the maxima for A_{xy} and A_{yx} , but suppressed compared to A_{zz} . The dashed vertical line marks the 2nd order P_z to B_\square phase transition.

A_{xx} , A_{yy} , A_{xy} and A_{yx} , become finite, signaling the transition to the B_\square phase. Close to the transition the B_\square phase is locally a “planar” phase deep within the channels due to the suppression of the orbital components normal to the boundary. However in the central region the B_\square phase is defined by all three diagonal components, as well as the off-diagonal components, A_{xy} and A_{yx} , allowed by D_{4h}^{L+S} symmetry.

6 Weak-Coupling Phase Diagram

The phase diagram for superfluid ^3He in the weak-coupling limit as a function of reduced temperature, T/T_c , and confinement length, D/ξ_0 , is shown in Fig. 4 for two values of the periodicity, $L = 5\xi_0$ (left panel) and $L = 20\xi_0$ (right panel). These two diagrams are qualitatively representative of the phase diagram for any $5 \leq L/\xi_0 \leq 30$. In particular, we do not find any additional equilibrium phases as minima of the GL functional with the weak-coupling material parameters.

The transition lines are found by classifying the phases based on non-negligible order parameter components, and then bracketing the location of both normal to P_z and the P_z to B_\square transitions. These brackets are refined until their width drops below a specified tolerance, which we chose to be $0.025\xi_0$. Note that predicted phase boundaries are limited by the restriction we place on the validity of the boundary condition for strong pair-breaking, i.e. $d \geq \xi_0/2$.

The phase boundary for the normal to P_z transition is determined by a linear eigenvalue equation, obtained by solving the linearized GL equation for the P_z order parameter, $\alpha(T)A_{zz} - K_1(\nabla_x^2 + \nabla_y^2)A_{zz} = 0$, within the domain V , and with boundary condition, $A_{zz}|_{\partial V} = 0$, for maximal pair-breaking. The eigenfunction, $A_{zz} \equiv a_1(x, y)$, corresponding to the highest instability temperature, T_{c1} , defines the spatial profile of the first unstable mode of the P_z phase. If we knew the exact

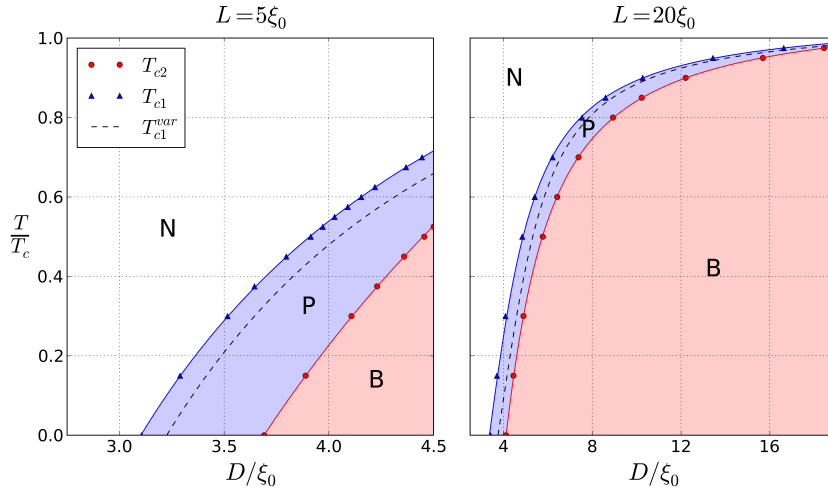


Fig. 4 (Color online) Phase diagrams for $L = 5\xi_0$ and $L = 20\xi_0$. The dashed curve is the normal to P_z transition obtained by the variational method. The solid curves are fits of the transition data points to the functional form of the variational curve. Note that there is a range of confinement lengths, D , for which only the P_z phase is realized.

functional form of the first unstable mode, $a_1(x, y)$, we could obtain the phase boundary, $T_{c_1}(D, L)$, from the equality in the Rayleigh-Ritz inequality,

$$\alpha(T_{c_1}) \geq \frac{-\int_V d\mathbf{R} \{K_1 |\nabla a(x, y)|^2\}}{\int_V d\mathbf{R} \{|a(x, y)|^2\}}. \quad (21)$$

In the absence of $a_1(x, y)$ we can obtain a lower bound on the N to P_z transition temperature with a good approximation to the eigenfunction $a_1(x, y)$. Consider the following approximation to the most unstable mode,

$$\begin{aligned} a(x, y) = & \left[\frac{C(x) + C(y)}{1 + C(x)C(y)} \right] \Theta(D/2 - |x|) \Theta(D/2 - |y|) \\ & + C(x) \Theta(D/2 - |x|) [\Theta(-D/2 - y) + \Theta(-D/2 + y)] \\ & + C(y) \Theta(D/2 - |y|) [\Theta(-D/2 - x) + \Theta(-D/2 + x)], \end{aligned} \quad (22)$$

where $C(x) = \cos(\pi x/D)$, $\Theta(x)$ is the Heaviside step function, and x and y are defined on the domain $[-L/2, L/2]$. This function is piece-wise continuous at the interfaces between the central region and the x - and y channels, and satisfies the strong pair-breaking boundary condition, $a|_{\partial V} = 0$. The variational result $T_{c_1}^{var}$, is shown in comparison to the exact numerical result for the $N - P_z$ phase boundary, T_{c_1} in Fig. 4.

For the range of $L \leq 30\xi_0$ that we consider, and for all $D \geq D_c(T)$ that gives a superfluid transition, the P_z phase is stable for a temperature range below T_{c_1} . Furthermore, for a given L there is a narrow range of confinement lengths, D , in

which only the P_z phase is stable. This is in sharp contrast to one-dimensional confinement in an infinite slab where the axial or planar phases are stable under strong confinement. The absence of these phases in the periodic confined geometry here is due to pair-breaking within the two orthogonal x and y channels, the large cost in gradient energy for x - and y orbital components for strong confinement and the weak-coupling β -parameters. Chiral phases, such as the A_{\square} -phase and the chiral- C_{4v} phase will be discussed in a separate report on GL theory of confined phases in the strong-coupling limit.

7 Conclusions

We have investigated the inhomogeneous phases of superfluid ^3He confined to a two-dimensional lattice of square, sub-micron-scale boundaries (“posts”) with translational invariance in the third dimension. In the weak-coupling limit, and strong pair-breaking by the boundary post, we find an instability from the normal state, at $T_{c_1} < T_c$ for bulk superfluid ^3He , to an equal-spin pairing state with z -aligned Polar orbital order. For fixed lattice spacing, L , there is a critical post dimension, d_c , above which only the periodic polar phase is stable. For $d < d_c$ we find a second, low-temperature phase onset at $T_{c_2} < T_{c_1}$ from the polar phase to a periodic “B-like” phase. The low temperature phase is inhomogeneous, anisotropic and preserves time-reversal symmetry, but unlike the bulk B-phase has only D_{4h}^{1+s} point symmetry. This or similar geometries may be realizable with current nano-fabrication processes, and could therefore provide a potential avenue for experimental studies of the polar phase in ^3He in well defined geometries.¹⁷ Further studies of ^3He in geometries with periodic confinement are expected to yield a large number of tunable phases with unique broken symmetries and topological properties that are not realized in bulk superfluid ^3He .

Acknowledgements This research is supported by the National Science Foundation (Grant DMR-1106315). We thank David Ferguson for many discussions and critique during the course of this work.

References

1. V. Ambegaokar, P. de Gennes, and D. Rainer, *Phys. Rev. A*, **9**, 2676 (1975).
2. D. Rainer and M. Vuorio, *J. Phys. C - Solid State Physics*, **10**, 3093 (1977).
3. P. de Gennes and D. Rainer, *Phys. Lett. A*, **46**, 429 (1974).
4. N. D. Mermin and T.-L. Ho, *Phys. Rev. Lett.*, **36**, 594 (1976).
5. P. M. Walmsley and A. I. Golov, *Phys. Rev. Lett.*, **109**, 215301 (2012).
6. T. Kunimatsu, H. Nema, R. Ishiguro, M. Kubota, T. Takagi, Y. Sasaki, and O. Ishikawa, *J. Low Temp. Phys.*, **171**, 280 (2013).
7. L. J. Buchholtz and G. Zwicknagl, *Phys. Rev.*, **B23**, 5788 (1981).
8. Y. Nagato, M. Yamamoto, and K. Nagai, *J. Low Temp. Phys.*, **110**, 1135 (1998).
9. A. Vorontsov and J. A. Sauls, *Phys. Rev. B*, **68**, 064508:1 (2003).
10. L. H. Kjälldman, J. Kurkijärvi, and D. Rainer, *J. Low Temp. Phys.*, **33**, 577 (1978).

-
11. A. B. Vorontsov and J. A. Sauls, *Phys. Rev. Lett.*, **98**, 045301 (2007).
 12. M. Freeman, R. S. Germain, E. V. Thuneberg, and R. C. Richardson, *Phys. Rev. Lett.*, **60**, 596 (1988).
 13. J. Xu and B. C. Crooker, *Phys. Rev. Lett.*, **65**, 3005 (1990).
 14. A. Schechter, R. W. Simmonds, R. E. Packard, and J. C. Davis, *Nature*, **396**, 554 (1998).
 15. L. V. Levitin, R. G. Bennett, A. Casey, B. Cowan, J. Saunders, D. Drung, T. Schurig, and J. M. Parpia, *Science*, **340**, pp. 6 (2013).
 16. M. Gonzalez, P. Zheng, E. Garcell, Y. Lee, and H. B. Chan, *Review of Scientific Instruments*, **84**, 025003 (2013).
 17. N. Zhelev, R. Bennett, R. Ilic, J. Parpia, L. Levitin, A. Casey, and J. Saunders, *Bulletin of the American Physical Society*, **58** (2013).
 18. D. Rainer and J. W. Serene, *Phys. Rev. B*, **13**, 4745 (1976).
 19. D. Vollhardt and P. Wölfle, *The Superfluid Phases of ^3He* (Taylor & Francis, New York, 1990).
 20. J. A. Sauls, *Phys. Rev. B*, **84**, 214509 (2011).
 21. E. V. Surovtsev and I. A. Fomin, *J. Low Temp. Phys.*, **150**, 487 (2008).
 22. O. C. Zienkiewicz, R. L. Taylor, and J. Z. Zhu, *The Finite Element Method: Its Basis and Fundamentals* (Butterworth-Heinemann, 2005).
 23. J. R. Shewchuk, in *Applied Computational Geometry: Towards Geometric Engineering*, Lecture Notes in Computer Science, Vol. 1148, edited by M. C. Lin and D. Manocha (Springer-Verlag, 1996) pp. 203–222.
 24. M. Abramowitz and I. A. Stegun, *Handbook of Mathematical Functions* (Dover, New York, 1970).
 25. W. W. Hager and H. Zhang, *ACM Transactions on Mathematical Software*, **32**, 113 (2006).